CORROSION SCIENCE AND TECHNOLOGY, Vol.31, No.4(2002), pp.291~298

Hydorgen Ion Transport through Aluminum Oxide Films by Cathodic Polarization in Hydrochloric Acid

Jong Hyun Seo and Dong Nyung Lee

School of Materials Science and Engineering, Seoul National University
Seoul 151-742, Korea

Hydrogen ion transport through the anodic aluminum oxide film by cathodic polarization was investigated by means of Elastic Recoil Detection Analysis (ERDA) with varying oxide film thickness. The proton conduction in barrier oxide film proved to follow the high field conduction theory and corresponding parameters were obtained from ERDA spectra. In addition, the possibility that accumulated hydrogen molecules at the metal/oxide interface can cause the blistering of the oxide film was deduced. Cracks along the peripheries of the blisters formed in the prior cathodic period act as new pit initiation sites in the subsequent anodic polarization.

Keywords *: proton transport, aluminum oxide, ERDA, blister, pit*

1. Introduction

It is well known that the anodic current flow through an aluminum barrier oxide film is very low until the potential exceeds the previous oxide formation potential. On the other hand, cathodic current for hydrogen evolution reaction is ready to flow at a relatively small cathodic overpotential in acid electrolytes.

This cathodic polarization behavior of aluminum has attracted many researchers investigating corrosion,[1-9] electrolytic coloring,[10-11] and especially pitting of aluminum in alternating current electrolytic etching in hydrochloric acid solution for electrolytic capacitor application.[12-20]

Cathodic conduction mechanisms are simply classified into two categories by hydrogen reduction site[21]: One is charge transport by electrons through barrier film and hydrogen evolution at the oxide/electrolyte interface and the other is charge transport by protons and hydrogen evolution at the metal/oxide interface. Identification of hydrogen evolution site and determination of the hydrogen transport amount through oxide film quantitatively are strongly relevant to breakdown mechanism of aluminum passivity such as hydration of surface oxide film,[1-8,17-19] cathodic corrosion of aluminum,[9,20] and blistering of oxide film[12] during cathodic polarization.

However, in the study of anodic aluminum oxide films, only few researchers have reported the hydrogen distribution and concentration within the anodic barrier aluminum oxide depending on anodizing conditions using SIMS,[22] NRA,[23] and XPS.[24] However, no attempt has been made to investigate the change of hydrogen contents in the oxide film by cathodic polarization with conventional detection methods.

In this work, the hydrogen ionic transport through the barrier oxide film was investigated using ERDA. The separation of proton current and electron current was possible from ERDA spectra and electrochemical transient curves. The high field conduction parameters of proton in the oxide film obtained by this method are in good agreement with published data. In addition, the morphological observations after the cathodic polarization were carried out using SEM and AFM.

2. Experimental

All specimens were cut from 800 μm thick cold rolled aluminum foil of 99.98% in purity.

Prior to anodizing, they were degreased in acetone and then electropolished in a mixture of perchloric acid and ethanol at 20V for 5 min. The barrier-type anodic oxide films were grown on the aluminum foil by anodizing in ammonium adipate solution at 60°C. Anodizing was conducted at a constant current of 0.5 mA/cm^2 initially until the anodizing voltage reached a desired value and switched to a constant voltage mode. The area of the foil exposed to the electrolyte was 3 cm^2. Polarization experiments of the anodized aluminum foils were performed using EG&G 273A potentiostat in 1M HCl acid solution at 30°C. A saturated calomel reference electrode (sce) was used and all potentials are referred to it in this paper.

The ERDA measurements were made to detect hydrogen within the oxide film on aluminum. The following experimental scattering parameters were used for this analysis: a 2.8MeV He^{++} ion beam was incident at 75° from the sample normal, the recoil atoms were transmitted through a 12 μm thick mylar foil and collected in a SBD over a solide angle of 2.5 msr at a scattering angle of 30° and a total incident fluence of 20 μC.

3. Results and discussion

3.1 Characterization of anodic oxide film by RBS and TEM

Fig. 1 shows the plane view of TEM image and diffraction pattern of stripped anodic oxide film formed at 25V in ammonium adipate solution. Electron diffraction patterns from stripped anodic films consisted of four or five very broad and diffuse rings, suggesting an amorphous structure. Corresponding TEM images at high magnification showed a fine grain-like morphology on the order of 2 nm. An ultramicrotomed section reveals a barrier layer oxide film of uniform thickness attached to the aluminum substrate. The thickness of the film is 44 nm.

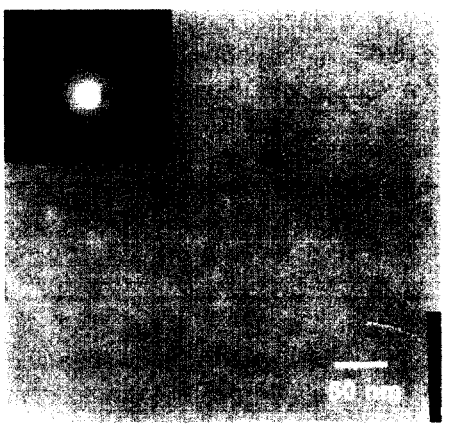

(a)

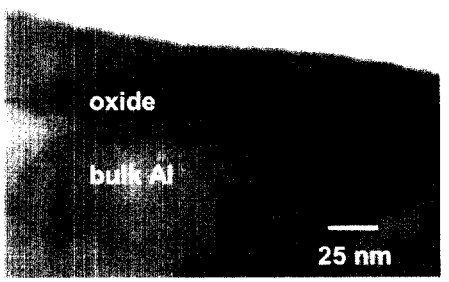

(b)

Fig. 1. TEM micrograph and deflection pattern of (a) plane view of stripped anodic oxide film and (b) ultramicrotomed section of anodic oxide film on aluminum formed to 25 V at 0.5mA/cm^2.

3.2 Cathodic polarization

Fig. 2 shows hydrogen reduction current as a function of applied cathodic potential in 1M HCl solution. The oxide thickness was approximately 40 nm. When the cathodic potential was maintained at -2V, the hydrogen reduction current density was less than 10 mA/cm^2 at 600sec. However, the current markedly increased at and above -2.5V, which was defined as the threshold potential in this work

The threshold potential was measured at varying oxide film thickness. The potential interval for measuring the threshold potential corresponding oxide thickness was 0.5 V. The potential shifted to more positive values with

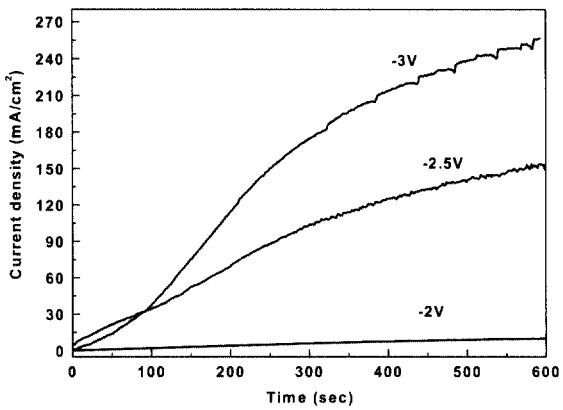

Fig. 2. Hydrogen reduction current of 40 nm thick oxide covered aluminum with different cathodic potentials in 1M HCl solution at 30℃

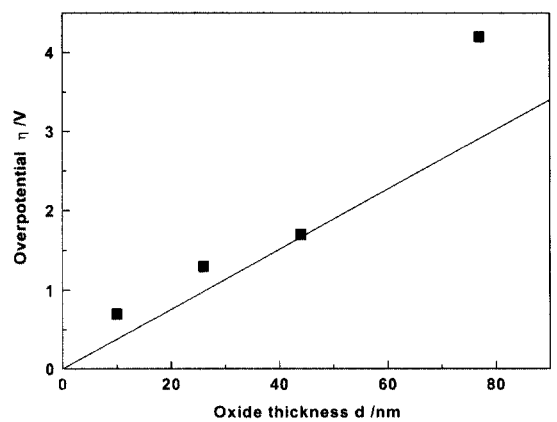

Fig. 3. Overpotential η in the oxide film as a function of oxide film thickness d.

decreasing oxide thickness. The overpotential (η) shown in Fig. 3 is the difference between the threshold potential and open circuit potential of the sample. In fact, the cell potential is comprised of three terms; overpotential at the metal/oxide, overpotential within the film, and IR drop due to solution resistance.[18] However, the solution resistance in this experiment is negligible. Hence, η is the sum of the overpotentials at the metal/oxide and within the film. The considerably large cathodic current starts to flow only when the electric field strength exceeds at least 4×10^5 V/cm (Fig. 3). This value is in agreement with the reported value for blister formation above pitting potential.[25] This value is much smaller than that of dielectric breakdown field strength of anodized aluminum oxide film, which lies between $1.5\sim7.0\times10^6$ V/cm.[26]

3.3 Elastic recoil detection analysis experiments

Proton migrating through the oxide film by electric field strength reduced into the form of hydrogen atom at the metal/oxide interface. The neutral hydrogen atom at the interface moves into the bulk aluminum substrate or outward to the electrolyte due to the hydrogen concentration difference. Throughout this work, the proton current is calculated from the ERDA results based on the hypothesis that the anodic oxide film on aluminum substrate acts as a diffusion barrier of hydrogen. The change of trapped hydrogen quantity in the sample is only affected by the hydrogen quantity formed at the metal/oxide interface via proton migration through the oxide film followed by reduction into hydrogen atom. The quantity of hydrogen detected in the sample represents the quantity of hydrogen reduced at the metal/oxide interface during the cathodic polarization. Permeation experiments reveal that the anodic oxide film on aluminum hinders hydrogen diffusion process.[27,28] It is therefore reasonable to assume that diffusion of the reduced hydrogen atoms into or outward the oxide film is negligible. The hydrogen atoms produced at metal/oxide interface diffuse more easily into defects of bulk aluminum such as vacancies and dislocations than lattice interstices.[29]

The hydrogen evolution current density transients and corresponding ERDA spectra for the anodized aluminum samples with different oxide thickness are shown in Fig. 4. In ERDA results, non-charged aluminum sample also exhibited some amount of hydrogen contents. The amount was 6.7×10^{22}/cm^3. This value lies within the range of reported values of the hydrogen concentration contained in various anodic aluminum oxide films.[22-24] Therefore, the channel 280 represents the metal/oxide interface. A remarkable result is that maximum hydrogen peak locates at the metal/oxide interface and hydrogen is also detected

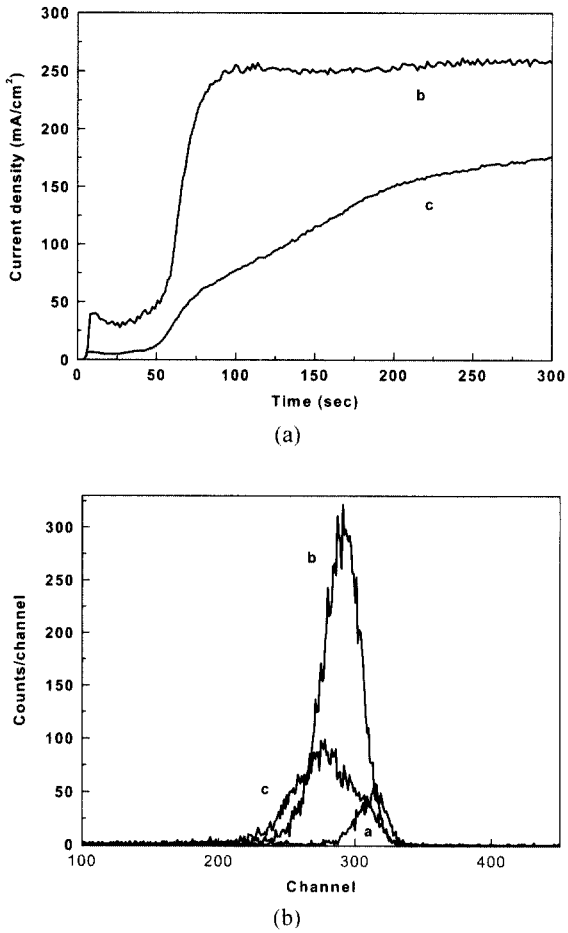

Fig. 4. (a) Hydrogen evolution current transient curves of anodized aluminum in 1M HCl polarized at -3V for 300sec, curve b 20 nm thick oxide and curve c 35 nm thick oxide; (b) corresponding ERDA spectra for curve a 20 nm thick oxide without cathodic polarization, curve b and c were the same condition as in (a).

inside the aluminum metal, when it was polarized at -3V for 300sec. This indicates that hydrogen accumulated at the metal/oxide interface due to proton conduction during the cathodic polarization.

The total cathodic current density (i_t) consists of electron transport current density and proton transport current density

$$i_t = i_e + i_p \quad (1)$$

where i_e and i_p represent electron transport and proton transport current densities, respectively.

The proton current density can be obtained from ERDA spectra. The areal density of hydrogen (ρ / atoms cm^{-2}), which is reduced at metal/oxide interface then remains in the sample, is obtained from the integrated area of ERDA spectrum.[33]

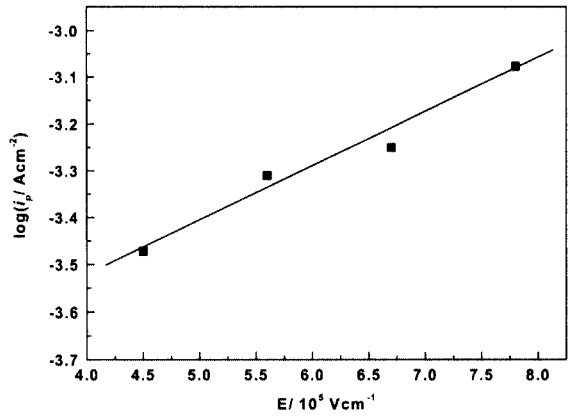

Fig. 5. Plot representing variation of proton transport current density i_p with electric field strength E in the film (i_p is calculated from ERDA)

The proton current density is obtained by following Eq. (2)

$$i_p = \frac{nF(\rho - \rho_o)}{N_a t} \tag{2}$$

where n is the number of electrons in the reaction, F is Faraday's constant, ρ_0 is the initial hydrogen areal density of anodic oxide film, N_a is the Avogadro number, and t is polarization time. For example, corresponding i_p of curve b in Fig.5 with the accumulated hydrogen density of 1.87×10^{18} atoms/cm^2 was 8.36×10^{-4} A/cm^2.

Fig. 5 shows the relation between the proton current density i_p and the electric field across the barrier oxide layer. The linearity indicates that the proton transport through the oxide film follows the high field conduction theory.

$$i_p = i_{po}\, exp(\beta E) \tag{3}$$

where β is the cathodic high-field conduction coefficient, E is the electric field strength in the oxide film. Eq. (3) may be modified to obtain a Tafel equations:

$$log\, i_p = log\, i_{po} + 0.4343\beta E \tag{4}$$

The conduction coefficient β is obtained from the slope of straight line. The slope and β are 1.19×10^{-6} and 2.76×10^{-6} cm/V, respectively. The value of i_{po} was 0.098 mA/cm^2, as E goes to zero. These values are good agreement with published data in.[18] They evaluated the values of β and i_{po} of aluminum covered with native oxide film in 0.1M HCl solution using cathodic tafel slopes. The reported values of β and i_{po} are 2.6×10^{-6} cm/V and 0.17 mA/cm^2, respectively.

To determine the portion of proton current to the total cathodic current with varying the oxide film thickness, the constant current experiments were conducted with different oxide thickness from 10 nm ~ 80 nm. The total cathodic charge passed was fixed at 8 C/cm^2 with constant cathodic current density of 20 mA/cm^2 for 400sec.

Fig. 6 shows the dependence potential-time curves on different oxide film thickness and their corresponding ERDA spectra. When a sudden current is applied to the oxide film, the charging of both sides of the oxide film builds up the electric field in the film due to dielectric property of aluminum oxide. The potential reached the maximum potential and decreased to a steady state potential with increasing charging time. The difference

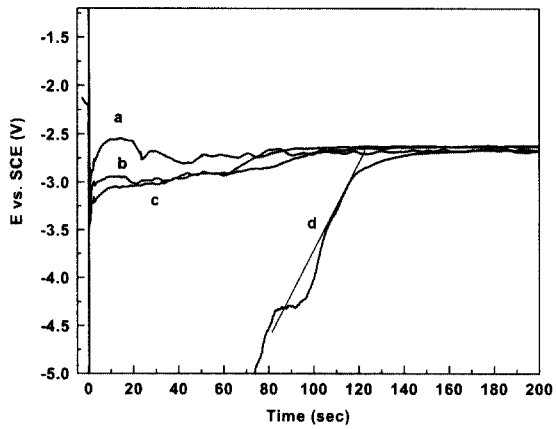

(a)

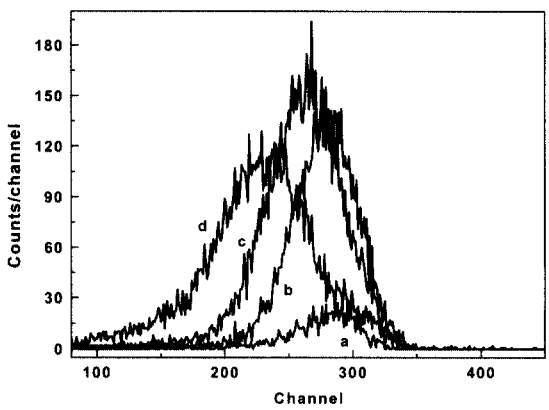

(b)

Fig. 6. Plots of (a) potential-time curves as a function of oxide film thickness at constant cathodic currrent density 20 mA/cm^2 for 400 sec and (b) corresponding ERDA specta. Curve a 10 nm, curve b 26 nm, curve c 44 nm, and curve d 77 nm. τ is time of middle point of slope.

Table 1. Summary of constant current density experiments with different oxide film thickness. Specimen numbers are the same in the Fig. 6.

Specimen	Initial oxide thickness(nm)	τ (sec)	ρ (10^{17}/cm^2)	Q_P (mC/cm^2)	Q_P/Q_t (%)
a	10	9	2.3	37.5	0.47
b	26	69	15.4	246	3.1
c	44	93	20.1	323	4.0
d	77	97	19.8	317	4.0

Q_t is total amount of cathodic charge: 8 C/cm^2.

between the maximum potential and OCP increased with increasing barrier oxide film thickness. The potential difference for a 77 nm thick oxide film was about 5V. This corresponds to an electric field of 6×10^5 V/cm in the film. However, when the time increased, the electric field in the film diminished to 2×10^5 V/cm.

The charge carried by proton and its ratio to total cathodic charge calculated from ERDA spectra are summarized in Table 1. τ is the transition time of potential from the maximum to the steady state value in the potential-time curve. Q_p represents the proton transport charge and is calculated from retained hydrogen amount in ERDA spectra.

Table 1 shows that for the more than 10nm thick oxide film, proton transport through the film occupies 3~4 % of total charge. The transition time is nearly proportional to the retained amount of hydrogen atoms. This implies that the proton transport conduction is dominant during the transition time. The ionic conduction is dramatically reduced to 0.5 % of total conduction at 10nm thick oxide film. It is the oxide film thickness that strongly affects the conduction mechanism in the film. The thinner is the oxide film, the more hydrogen evolution takes place at the oxide/electrolyte interface via electron transport conduction. This resulted in the reduction of retained hydrogen amount of the sample in ERDA measurement after cathodic polarization. Electronic transport in barrier oxide film may occur as resonance tunnelling or direct elastic tunneling.[31] The tunnelling process is strongly related to barrier layer thickness. The resonance tunnelling is likely to happen in a relatively thick oxide film above 10nm. On the other hand, if the oxide film thickness is thinner than 10nm, the direct elastic tunnelling is preferred conduction mechanism.

3.4 Blister observation after cathodic polarization

It is clear from the ERDA experiments that hydrogen accumulated at the metal/oxide interface due to ionic conduction through the oxide film during cathodic polarization and hydrogen evolution at the metal/oxide interface by proton conduction preferred in the relatively thick oxide film rather than thin one. Based on this result, the blistering of thick oxide film during cathodic polarization is explained as follows.

When the electric field in the oxide film exceeds a critical value, a great deal of proton migrates through the aluminum oxide and reduced into hydrogen atom at the metal/oxide interface according to the following reaction:

$$H^+ + e^- \rightarrow H \qquad (5)$$

The formation of the hydrogen molecule may be either a reaction of the type of electrochemical desorption or a combination of two hydrogen atoms. These hydrogen bubbles cannot easily diffuse out of the film due to relatively low diffusivity in the oxide film and their relatively large size compared to that of pathway such as fissures and flaws in the film. If small bubbles are in contact with the boundary of a large bubble, they diffuse into larger one to reduce their energy ($G = 2\gamma/r$ with γ and r being the surface tension and radius of a bubble, respectively). If the accumulation amount of hydrogen at the metal/oxide is sufficiently high enough to overcome the adhesion force of the oxide/metal interface, the mechanical breakdown of the oxide film can occur as a form of blistering or rupture of it. This exposes the bare substrate surface to electrolyte, accelerating the reduction of hydrogen ions.

Blisters in the oxide film were observed after cathodic polarization as shown in Fig. 7. Blisters generally had the circular shape. The blisters were observed only if the working electrode potential maintained by the potentiostat was below the threshold potentials as indicated in Fig. 3. For example, in 1M HCl solution, 40nm thick oxide with the potential set below -2.5V of duration of 10sec yielded blisters. The average radius of blisters ranged 10~15 μm for an oxide thickness below 50 nm. As the oxide thickness increased above 50 nm, only few blisters were observed and the measured radius steeply dropped to 1 μm. A ruptured blister is shown in fig. 7 (b). In contrast to the result,[32] the initiation of rupture was not at the center but the periphery of the blister. This might be ascribed to the strain concentration in the periphery of the oxide film during the blister growth. The number of ruptured blisters observed under the optical microscope and atomic force microscope was much smaller than under SEM, because they were ruptured more easily in a vacuum system of SEM.

AFM image of the blister is presented in fig. 8. This blister was obtained by cathodic polarization at -3V for 10sec in 1M hydrochloric acid solution. The oxide film

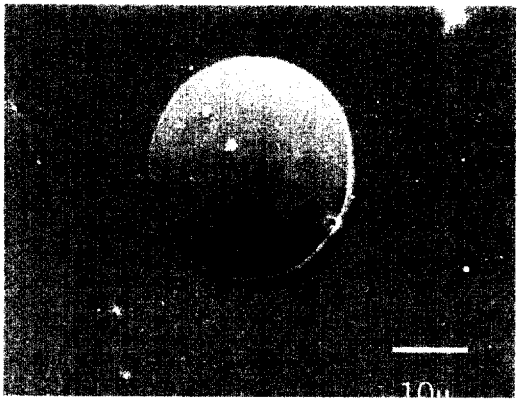

(a)

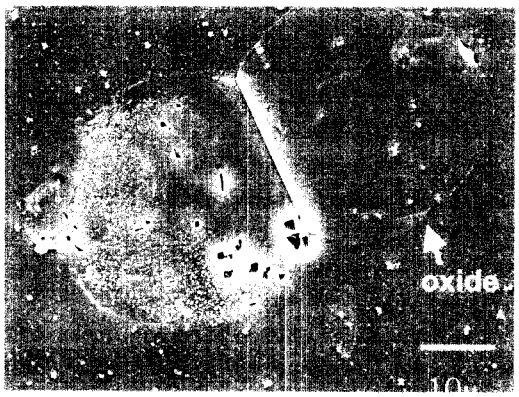

(b)

Fig. 7. SEM micrographs of (a) blisters formed on aluminum surface after cathodic polarization at -3V for 10 s and (b) pits formed after removal of blister. Oxide film thickness is about 40 nm.

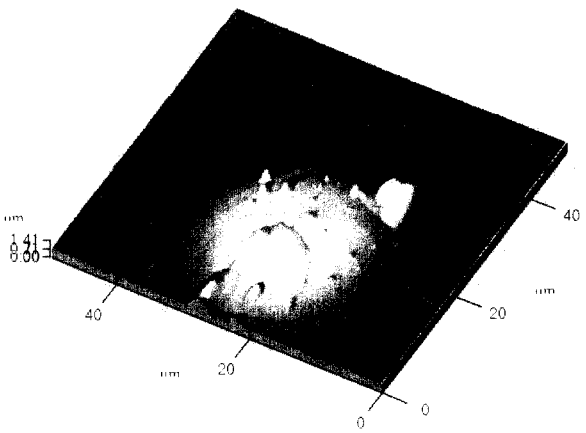

Fig. 8. Atomic force micrograph showing blister formed on aluminum surface covered with 40 nm thick oxide film after cathodic polarization at -3V for 10 s in 1M HCl at 30℃.

thickness is about 40nm. It was somewhat difficult task to obtain the clear image of the blister in the AFM, because most of them collapsed and lost their initial hemispherical shape due to a load of the cantilever and sudden change of the height of the blister during the contact image scanning of AFM. The precipitates composed of aluminum and oxygen (from EDS analysis) are shown on the outer surface of the blister.

The blister formation and rupture often observed in the pitting of aluminum and other alloys. Blistering of the oxide film of aluminum and its alloys has been reported.[25,32-34] These blisters formed above pitting potential are interpreted as a precursor of pitting[25] or by-products such as occluded cell of pit.[32-34]

In this work, the blisters were also found at cathodic polarization much below the pitting potential of anodized aluminum in hydrochloric acid solution. The cathodically formed blister differed from anodically formed ones. In

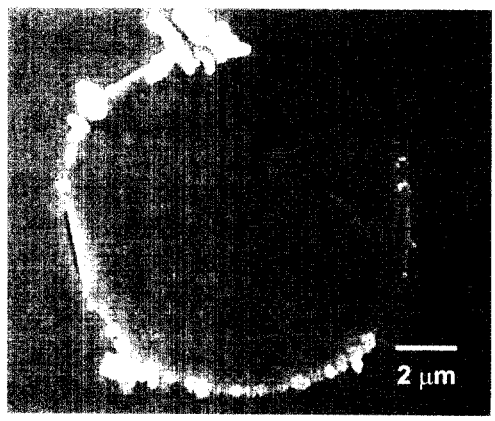

(a)

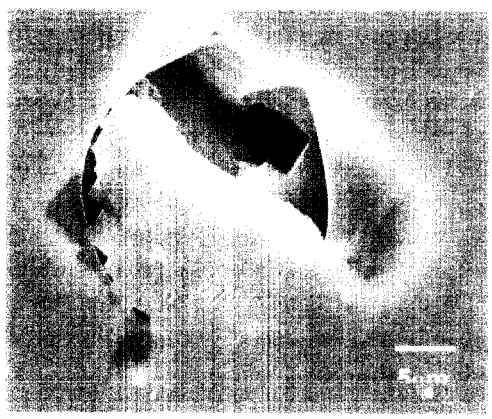

(b)

Fig. 9. SEM micrographs showing (a) cracking after cathodic polarization and (b) pit in subsequent anodic polarization at periphery of blister in 1M HCl. 10 nm thick oxide film, cathodic polarization -3V for 10 s, anodic polarization -0.5V for 0.1s.

pit, this means that the blisters produced by cathodic physical appearance, it did not accompany with underlying polarizaition were not the by-product of pit propagation process. Moreover, the results indicate that these blisters directly engaged to pitting and they supplied the new pit initiation sites when the specimen was subjected to anodic polarization above the pitting potential. Fig. 9 shows the evidence for such a possibility. A number of etch pits nucleated and propagated along the periphery of the blister formed by cathodic polarization due to crack initiation along the periphery. During cathodic polarization, a blister initiated at A indicated in fig. 9 (b) and grew laterally until internal hydrogen pressure exceeded the critical rupture stress. Crack initiated at the periphery of the blister and the electrolyte containing the chloride ion contacted the aluminum bare surface. During the following anodic polarization, the bare surface along the periphery of the blister was likely to dissolve. The (100) crystallographic cubic etch pits well developed at the periphery of the blister.

4. Conclusions

The change of the amount of hydrogen retained in aluminum covered with anodic oxide film due to cathodic polarization was investigated using by ERDA and the following results were obtained.

1) The high field conduction parameters for transport of proton through the oxide film were obtained from the hydrogen areal densities of ERDA.

2) The portion of ionic current in the total cathodic current increased with oxide thickness under the constant current condition. When the oxide film thickness reduced to 10 nm, only 0.5% of the total cathodic charge was carried by protons.

3) The blistering of oxide film during cathodic polarization was attributed to hydrogen atoms accumulated in the metal/oxide interface. The periphery of the blister formed in the prior cathodic period was the preferred pit nucleation site in the subsequent anodic polarization.

Acknowledgement

This study has been supported from NRL for texture control, Seoul National University.

References

1. K. Nisancioglu and H. Holtan, *Corros. Sci.* **19**, 537 (1979).
2. A. R. Despic, J. Radosevic, P. Dabic, and M. Kliskic, *Electrochim. Acta,* **35**, 1743 (1990).
3. J. Radosevic, M. Kliskic, P. Dabic, R. Stevanovic, and A. Despic, *J. Electroanal. Chem.*, **277**, 105 (1990).
4. A. R. Despic, D. M. Drazic, J. Balaksina, LJ. Gajic-Krstajic, and R. M .Stevanovic, *Electrochim. Acta*, **35**, 1747, (1990).
5. S.-M. Moon and S.-I. Pyun, *Corrosion*, **54**, 546, (1998).
6. K. Nisancioglu and H. Holtan, *J. Electrochem. Soc.*, **24**, 1229 (1979).
7. J. Kunze, *J. Electrochem. Soc.*, **7**, 273 (1967).
8. J. Radosevic, M. Kliskic, P. Dabic, R. Stevanovic, and A. Despic, *J. Electroanal. Chem.*, **277**, 105 (1990).
9. E. P. G. T. Van De Ven and H. J. Koelmans, *J. Electrochem. Soc.*, **123**, 143 (1976).
10. A. S. Doughty, G. E. Thompson, J. A. Richardson, and G. C. Wood, *Trans. Inst. Metal Finishing*, **53**, 33 (1975).
11. K. Yanagida, T. Hirokane, T. Tsuyukiyasu, and T. Sato, *J. Metals*, 1976, 3, (1976)
12. J. H. Seo, S.-Y. Jeong, H.-J. Shin, and D. N. Lee, in *Proceedings of the 2nd Aluminum Surface Science and Technology*, Manchester, 2000, in press.
13. J. H. Jeong, S. S. Kim, H. G. Kim, C. H. Choi, D. N. Lee, *Materials Science Forum*, **217**, 1565 (1996).
14. K. Vu. Quang and F. J. Brindel, *J. Electrochem. Soc.*, **130**, 1248 (1983).
15. C. K Dyer and R. S. Alwitt, *J. Electrochem. Soc*, **128**, 300 (1981).
16. C.-F. Lin and K. R. Hebert, *J. Electrochem. Soc.*, **137**, 3723 (1990).
17. C.-F. Lin, M. D. Porter, and K. R. Hebert, *J. Electrochem. Soc.*, **141**, 96 (1994).
18. C.-F. Lin and K. R. Hebert, *J. Electrochem. Soc.*, **141**, 104 (1994).
19. M.- H. Wang and K.R. Hebert, *J. Electrochem. Soc.*, **143**, 2827 (1996).
20. H. Terryn, J. Vereecken and G. E. Thompson, *Corros. Sci.* **32**, 1173 (1991).
21. A. W. Hassel and M.M. Lohrengel, *Electrochim. Acta*, **40**, 433 (1995).
22. M.F. Abd Rabbo, J.A. Richardson and G.C. Wood, *Electrochim. Acta*, **22**, 1375 (1977).
23. W. A. Lanford, R. S. Alwitt, and C. K. Dyer *J. Electrochem. Soc.*, **127**, 405 (1980).
24. H. Takahashi, K. Fujimoto, H. Konno, and M. Nagayama, *J. Electrochem. Soc.*, **131**, 1856, (1984).
25. C. B. Bargeron and R. B. Givens, *J. Electrochem. Soc.*, **124**, 1845 (1977).
26. L. L. Hench and D. B. Dove, in *Physics of electronic ceramics*, part A, Marcel Dekker, Inc., New York, 541 (1971).
27. A. Csanady, K. Papp, and E. Pasztor, *Mater. Sci. Engng.* , **48**, 35 (1981).
28. W. Song, J. Du, Y. Xu, and B. Long, *J. Nucl, Mater.*, **246**, 139 (1997).
29. G. A. Young JR and J. R. Scully, *Acta. Mater.*, **46**, 6337 (1998).
30. J. R. Tesmer and M. Nastasi, in *Handbook of modern ion beam materials analysis*, MRS, Pittsburgh, Pennsylvania. 93 (1999).

31. R. H. Bube, in *Electrons in Solids*, Academic press, Inc., New York, 239 (1992).
32. P. M. Natishan and E. McCafferty, *J. Electrochem. Soc.*, **136**, 53 (1989).
33. R. L. Ryan and E. McCafferty, *J. Electrochem. Soc.*, **142**, 2594 (1995).
34. J. Perkins, J. R. Cummings, and K. J. Graham, *J. Electrochem. Soc.*, **129**, 137 (1982).